International Journal of
Molecular Sciences

MDPI

Article

Gut Microbiota-Derived Metabolites in Oligozoospermia and Asthenozoospermia: Exploring Molecular Mechanisms Through Network Pharmacology and Molecular Docking

Quanxin Su, Yingwei Bi, Kenan Wang, Weiwei Fan and Jianbo Wang *

Department of Urology, The First Affiliated Hospital of Dalian Medical University, 116000 Dalian, China; su18340860412@163.com (Q.S.)
* Correspondence: wangjianbo@dmu.edu.cn

Abstract

This study explored the potential molecular associations of gut microbiota-derived metabolites with oligozoospermia and asthenozoospermia and identified key candidate targets, pathways, and microbiota–substrate–metabolite–target relationships. Human gut microbiota, substrates, metabolites, and host genes were obtained from gutMGene. Metabolite targets were predicted using SwissTargetPrediction and SEA, while disease-related targets were collected from GeneCards, OMIM, and CTD. Candidate targets were identified by intersection analysis. Protein–protein interaction networks were constructed to prioritize highly connected candidate targets, followed by GO and KEGG enrichment analyses. SwissADME and ADMETlab were used to characterize physicochemical properties and predict toxicity, respectively. An M-S-M-T network was constructed, and molecular docking was performed to assess potential metabolite–target interactions. In total, 1518 gut microbiota metabolite-related targets were obtained, yielding 22 candidate targets for oligozoospermia and 17 for asthenozoospermia. CXCL8, IL6, TNF, and TP53 were identified as shared highly connected candidate targets. GO analysis indicated enrichment in responses to bacterial-origin molecules, lipopolysaccharide response, inflammation, cytokine activity, and redox homeostasis. KEGG analysis highlighted MAPK, PI3K-Akt, TNF, HIF-1, and cytokine–cytokine receptor interaction pathways. The M-S-M-T network suggested a potential association involving *Clostridium sporogenes*, tyrosine/phenylalanine-derived aromatic metabolites, and CXCL8, based on the integration of reported microbial metabolic relationships and predicted metabolite–target interactions. Molecular docking yielded predicted binding scores for 3-phenylpropionic acid and 4-hydroxyphenylacetic acid with CXCL8. This network pharmacology study identified CXCL8, IL6, TNF, and TP53 as candidate targets potentially linking gut microbiota-derived metabolites with oligozoospermia and asthenozoospermia. The predicted associations involving aromatic metabolites and CXCL8 provide hypotheses for further investigation. Experimental and clinical validation is required to determine whether these associations have biological relevance in male reproductive dysfunction.

Keywords: gut microbiota; metabolites; CXCL8; oligozoospermia; asthenozoospermia; network pharmacology; molecular docking

Academic Editor: Elisabetta Baldi

Received: 07 October 2026
Revised: 07 November 2026
Accepted: 09 November 2026
Published: 18 November 2026

Copyright: © 2026 by the authors. Licensee MDPI, Basel, Switzerland. This article is an open access article distributed under the terms and conditions of the Creative Commons Attribution (CC BY) license.

1. Introduction

Male infertility is an important reproductive health problem affecting people of reproductive age. Male factors, either alone or together with female factors, contribute to approximately 30–50% of infertility cases [1,2]. Among these factors, oligozoospermia and asthenozoospermia are common semen abnormalities characterized by reduced sperm concentration and impaired sperm motility, respectively, with the sixth edition of the WHO laboratory manual reporting lower fifth-percentile reference values of 16×10^6/mL for sperm concentration, 42% for total motility, and 30% for progressive motility [3]. Their occurrence is associated with multiple factors, including genetics, endocrine disorders, urogenital infection, environmental exposure, and lifestyle; however, the etiology remains unclear in some patients [4–6]. Oxidative stress and chronic inflammation are considered important pathological mechanisms. Excessive reactive oxygen species can cause sperm membrane lipid peroxidation, mitochondrial dysfunction, and DNA damage, whereas abnormal inflammatory cytokine levels can disrupt the blood–testis barrier and the spermatogenic microenvironment and induce germ cell apoptosis [7–9].

The gut microbiota plays an important role in maintaining host health, and alterations in its composition and metabolic activity have been associated with various pathological conditions, including obesity, type 2 diabetes, inflammatory bowel disease, and neurological disorders [10,11]. The gut microbiota is involved in host metabolism, immune regulation, and inflammatory responses, and its metabolites can also affect the function of distant organs. In recent years, increasing attention has been paid to the gut microbiota–testis axis and its potential role in male reproductive health. Through the production of short-chain fatty acids, tryptophan and indole derivatives, and aromatic amino acid metabolites, the gut microbiota may influence systemic inflammation, hormone metabolism, and reproductive function [12,13]. Clinical studies have shown abnormalities in the microbial composition of the gut, urine, and semen in male infertility; in patients with asthenozoospermia, gut microbial diversity is decreased, and several differentially abundant genera are significantly associated with sperm motility [14,15]. Animal studies have further demonstrated that high-fat diet-induced dysbiosis can impair spermatogenesis and sperm motility, whereas fecal microbiota transplantation or remodeling of beneficial microbial communities can improve testicular tissue status and semen quality, suggesting that the gut microecology may be involved in male reproductive dysfunction [16–18].

Although existing studies suggest a close association between the gut microbiota and male infertility, most have focused on differences in microbial composition or the effects of single metabolites. A systematic analysis integrating reported and predicted microbiota–substrate–metabolite–host target relationships is still lacking. Network pharmacology can integrate information on metabolite targets, disease genes, protein interactions, and signaling pathways, making it suitable for revealing complex mechanisms involving multiple components, targets, and pathways [19]. Therefore, this study aimed to identify candidate targets associated with gut microbiota-derived metabolites in oligozoospermia and asthenozoospermia separately and to explore their shared molecular features. To achieve this, we integrated data from gutMGene, SwissTargetPrediction, SEA, GeneCards, OMIM, and CTD, followed by PPI network analysis and GO and KEGG enrichment analyses to identify shared highly connected candidate targets and relevant signaling pathways. We further constructed microbiota–substrate–metabolite–target (M-S-M-T) networks and performed molecular docking to explore potential interactions between representative aromatic metabolites and candidate targets.

2. Results

2.1. Screening of Candidate Targets Potentially Associated with Gut Microbiota-Derived Metabolites in Oligozoospermia and Asthenozoospermia

Following compound structure matching, 226 metabolites with PubChem identifiers and SMILES information were included in target prediction. Integration of the SwissTargetPrediction and SEA results yielded 1518 unique metabolite-related targets (Supplementary Table S1). Disease-related targets from GeneCards, OMIM, and CTD were then integrated, yielding 1205 targets related to oligozoospermia and 549 targets related to asthenozoospermia. For oligozoospermia, the metabolite-related targets, disease-related targets, and gutMGene human host genes were intersected, resulting in 22 candidate targets, including AHR, AKT1, APP, CASP3, CXCL8, CYP1A1, EGFR, IL6, TNF, TP53, and VEGFA (Figure 1). For asthenozoospermia, the same strategy identified 17 candidate targets, including CASP3, CXCL8, GSK3B, HDAC11, IL1B, IL6, MAPK1, MAPK14, NFKB1, TNF, TP53, and VEGFA (Figure 2). The two diseases shared 12 overlapping candidate targets, including CXCL8, IL6, TNF, and TP53. This overlap suggests that the two conditions may involve common molecular processes related to inflammatory responses, oxidative stress, and cellular injury, providing a basis for the subsequent comparison of their PPI networks. Sensitivity analysis using alternative SwissTargetPrediction, SEA, and GeneCards filtering criteria revealed variable sensitivity of candidate target selection, with a particularly pronounced effect of the GeneCards Relevance Score threshold. Detailed results are provided in Supplementary Table S6.

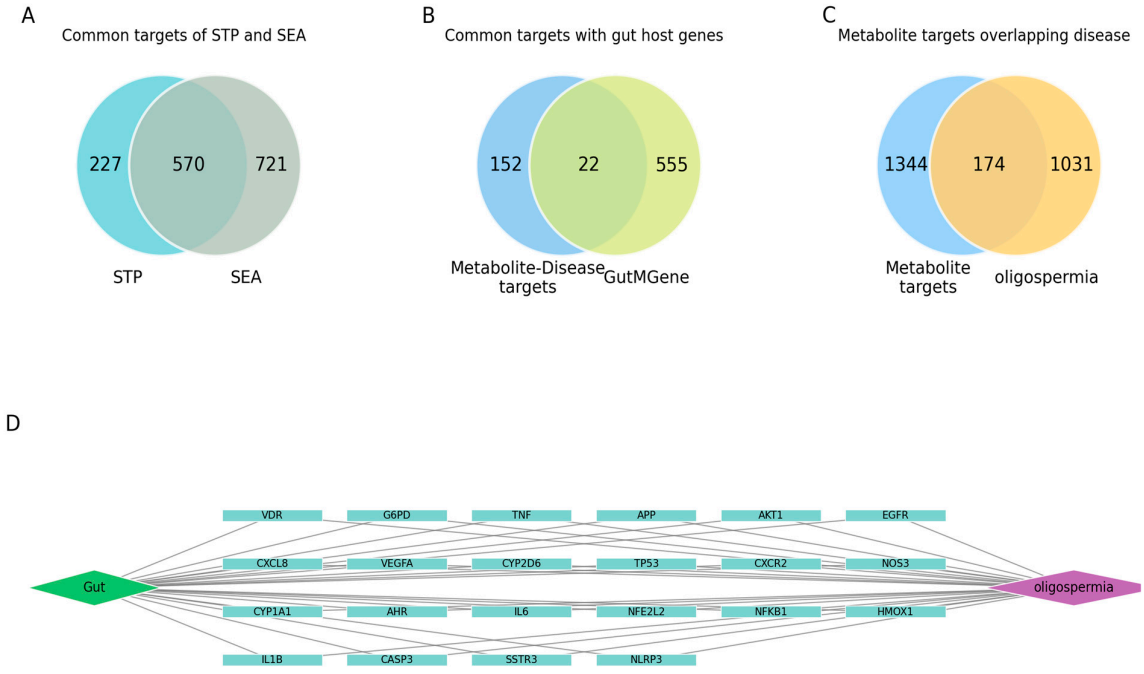


Figure 1. Screening of candidate targets potentially associated with gut microbiota-derived metabolites and oligozoospermia. (**A**): intersection of targets predicted by SwissTargetPrediction and SEA; (**B**): intersection between gut microbiota metabolite-oligozoospermia overlapping targets and gutMGene host genes; (**C**): intersection between gut microbiota metabolite targets and oligozoospermia disease targets; (**D**): Gut–Target–Oligozoospermia regulatory network.

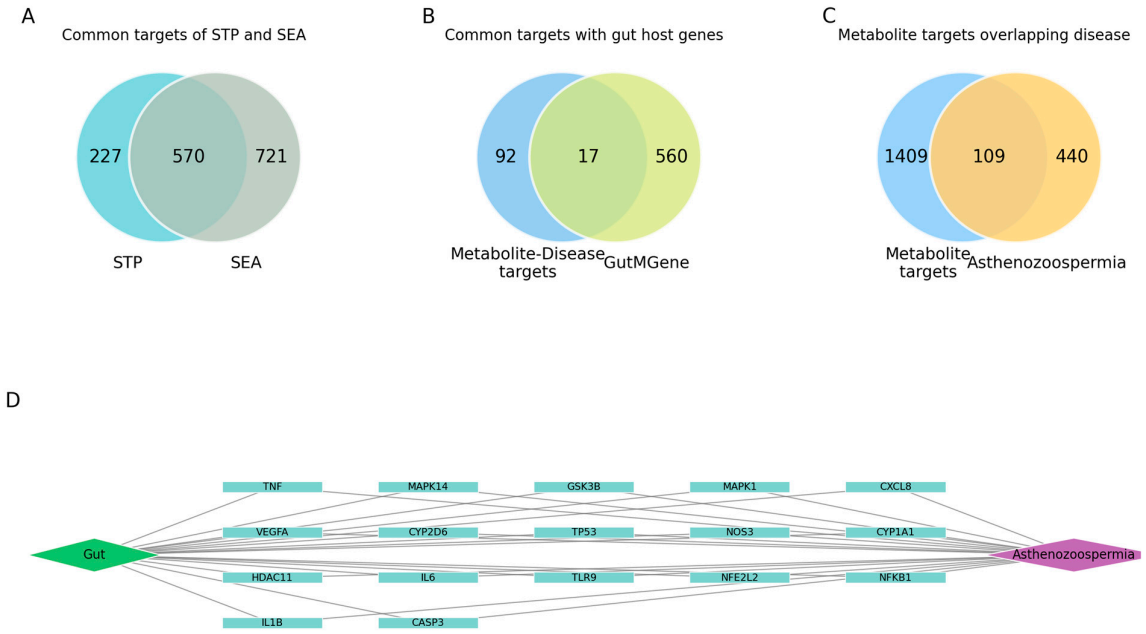


Figure 2. Screening of candidate targets potentially associated with gut microbiota-derived metabolites and asthenozoospermia. (**A**): intersection of targets predicted by SwissTargetPrediction and SEA; (**B**): intersection between gut microbiota metabolite-asthenozoospermia overlapping targets and gutMGene host genes; (**C**): intersection between gut microbiota metabolite targets and asthenozoospermia disease targets; (**D**): Gut–Target–Asthenozoospermia regulatory network.

To evaluate the influence of the gutMGene host gene filter, we compared candidate target sets obtained with and without this additional restriction. Without the gutMGene filter, 174 and 109 candidate targets were identified for oligozoospermia and asthenozoospermia, respectively. Applying the filter reduced these sets to 22 and 17 targets, indicating substantial dependence of candidate target selection on this prioritization step. CXCL8, IL6, TNF, and TP53 were present in both the filtered and unfiltered candidate sets. Detailed results are provided in Supplementary Table S7.

2.2. PPI Network Construction and Candidate Target Prioritization

Candidate targets were imported into the STRING database to construct protein–protein interaction (PPI) networks, followed by topological analysis in Cytoscape. The oligozoospermia PPI network contained 22 nodes and 130 interaction edges, whereas the asthenozoospermia PPI network contained 17 nodes and 83 interaction edges. Highly connected candidate nodes were initially prioritized according to DC values. IL6, TNF, AKT1, CXCL8, and TP53 were the five highest-degree nodes in the oligozoospermia network. In the asthenozoospermia network, CXCL8, IL6, TNF, and TP53 had DC values of 14, whereas CASP3 and IL1B both had DC values of 13. Because CASP3 and IL1B were tied at the selection boundary, both were retained, resulting in six highly connected candidate nodes. Additional analyses using BC, CC, and MCC showed substantial overlap with the DC-based selection, particularly for CC and MCC, while BC highlighted additional nodes such as CYP1A1. Notably, CASP3 and IL1B exhibited identical values across all four topological metrics (Table 1; Figure 3). The shared highly connected candidate targets of the two diseases were CXCL8, IL6, TNF, and TP53, suggesting that inflammatory cytokines, chemotactic signaling, and cellular stress-related molecules may

represent common molecular features associated with oligozoospermia and asthenozoospermia in the context of gut microbiota-derived metabolites. AKT1 was more prominent in the oligozoospermia network, whereas CASP3 was more prominent in the asthenozoospermia network, suggesting potentially different patterns of involvement of cell survival- and apoptosis-related proteins in the two conditions.

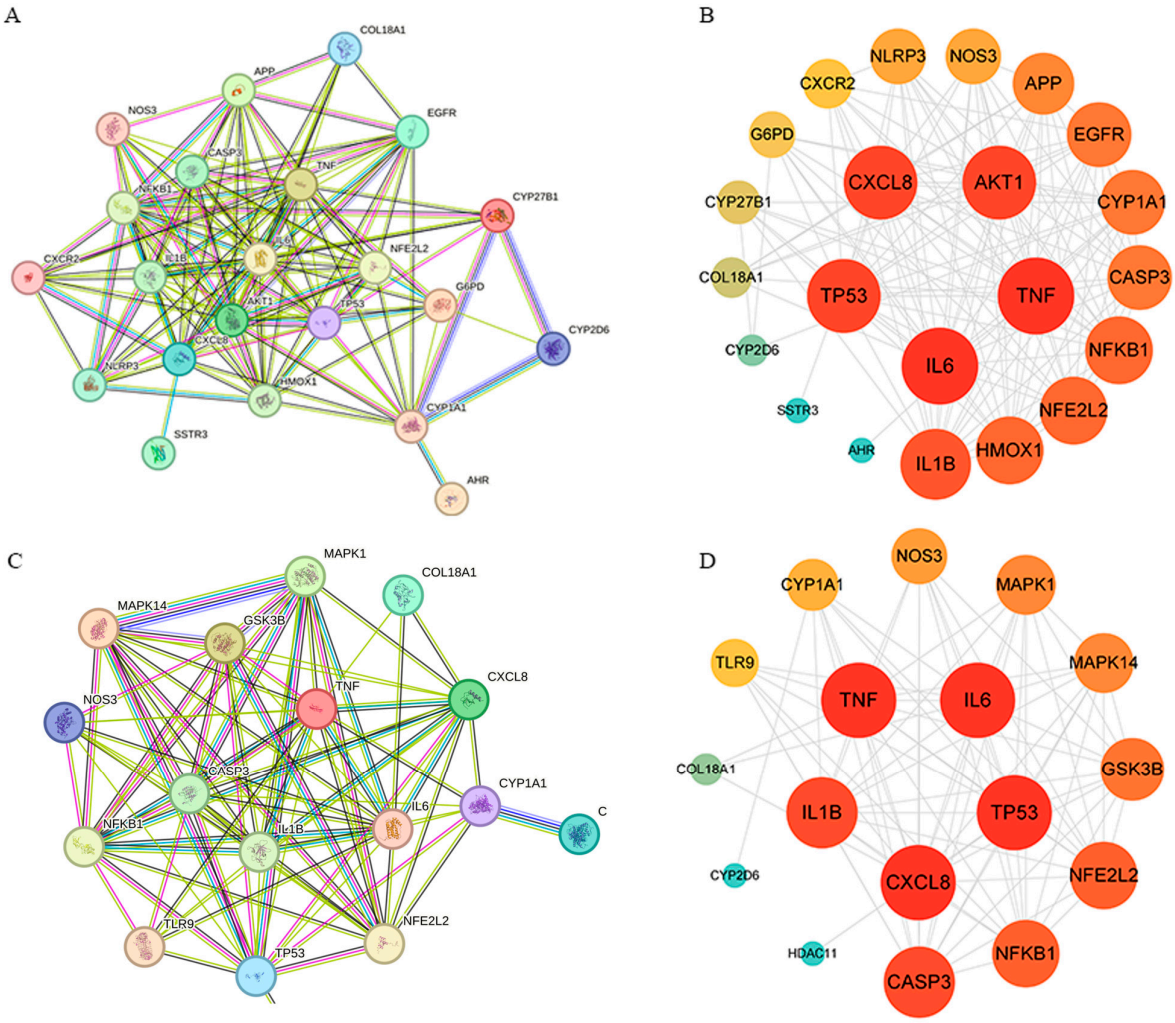


Figure 3. PPI networks and candidate target prioritization for oligozoospermia and asthenozoospermia. (**A**,**B**): STRING PPI network and Cytoscape-style network for oligozoospermia; (**C**,**D**): STRING PPI network and Cytoscape-style network for asthenozoospermia. Node size and color intensity reflect network degree, and red nodes indicate the highly connected candidate targets prioritized in each PPI network.

Table 1. Topological characteristics of nodes in the oligozoospermia and asthenozoospermia PPI networks.

Oligozoospermia Target	DC	BC	CC	MCC	Asthenozoospermia Target	DC	BC	CC	MCC
IL6	18	0.04622	0.87500	87,177,840	CXCL8	14	0.05860	0.88889	4,001,766
TNF	18	0.04622	0.87500	87,177,840	IL6	14	0.05860	0.88889	4,001,766
AKT1	17	0.03205	0.84000	87,177,600	TNF	14	0.05860	0.88889	4,001,766
CXCL8	17	0.11645	0.84000	87,172,561	TP53	14	0.14749	0.88889	4,001,761
TP53	17	0.03106	0.84000	87,177,120	CASP3	13	0.02249	0.84211	4,001,760
IL1B	16	0.02134	0.80769	87,172,080	IL1B	13	0.02249	0.84211	4,001,760
HMOX1	15	0.01373	0.77778	87,096,240	NFE2L2	12	0.01376	0.80000	3,996,720
NFE2L2	15	0.01373	0.77778	87,096,240	NFKB1	12	0.00780	0.76190	3,996,720
NFKB1	15	0.01505	0.75000	83,543,160	GSK3B	11	0.00185	0.72727	3,991,680
CASP3	14	0.00646	0.75000	87,091,200	MAPK1	10	0.00000	0.69565	3,628,800
CYP1A1	14	0.14950	0.75000	3,633,965	MAPK14	10	0.00000	0.69565	3,628,800
EGFR	14	0.01398	0.75000	43,586,640	NOS3	9	0.00000	0.66667	362,880
APP	13	0.00615	0.67742	79,834,320	CYP1A1	8	0.12500	0.66667	5041
NLRP3	11	0.00159	0.63636	3,669,120	TLR9	7	0.00000	0.61538	5040
NOS3	11	0.00000	0.63636	39,916,800	COL18A1	3	0.00000	0.51613	6
CXCR2	9	0.00043	0.60000	80,640	CYP2D6	1	0.00000	0.41026	1
G6PD	8	0.01874	0.60000	5042	HDAC11	1	0.00000	0.48485	1
CYP27B1	7	0.01873	0.58333	242					
COL18A1	6	0.00000	0.55263	720					
CYP2D6	3	0.00095	0.46667	4					
AHR	1	0.00000	0.43750	1					
SSTR3	1	0.00000	0.46667	1					

Notes. DC, degree centrality; BC, normalized betweenness centrality; CC, closeness centrality; MCC, maximal clique centrality. MCC was calculated as the sum of $(|C| - 1)!$ over all maximal cliques C containing each node. All metrics were computed from the original STRING interaction lists as undirected, unweighted networks. BC and CC are reported to five decimal places; MCC values are reported as integers.

2.3. GO Functional Enrichment Analysis

GO enrichment analysis showed that candidate targets for oligozoospermia were mainly enriched in biological processes such as oxidative stress, chemical stress, lipopolysaccharide response, response to molecule of bacterial origin, and cellular response to biotic stimulus. Cellular components mainly included membrane raft, membrane microdomain, vesicle lumen, and transcription regulator complex. Molecular functions mainly included cytokine receptor binding, cytokine activity, monooxygenase activity, and oxidoreductase activity (Figure 4A,B). Candidate targets for asthenozoospermia were mainly enriched in biological processes such as response to molecule of bacterial origin, cellular response to biotic stimulus, lipopolysaccharide response, and tumor necrosis factor response. Cellular components mainly included secretory granule lumen, cytoplasmic vesicle lumen, membrane raft, and vesicle lumen. Molecular functions mainly included cytokine receptor binding, cytokine activity, protease binding, and growth factor receptor binding (Figure 4C,D). Responses to molecules of bacterial origin, inflammatory regulation, and redox homeostasis may therefore represent key biological processes shared by oligozoospermia and asthenozoospermia.

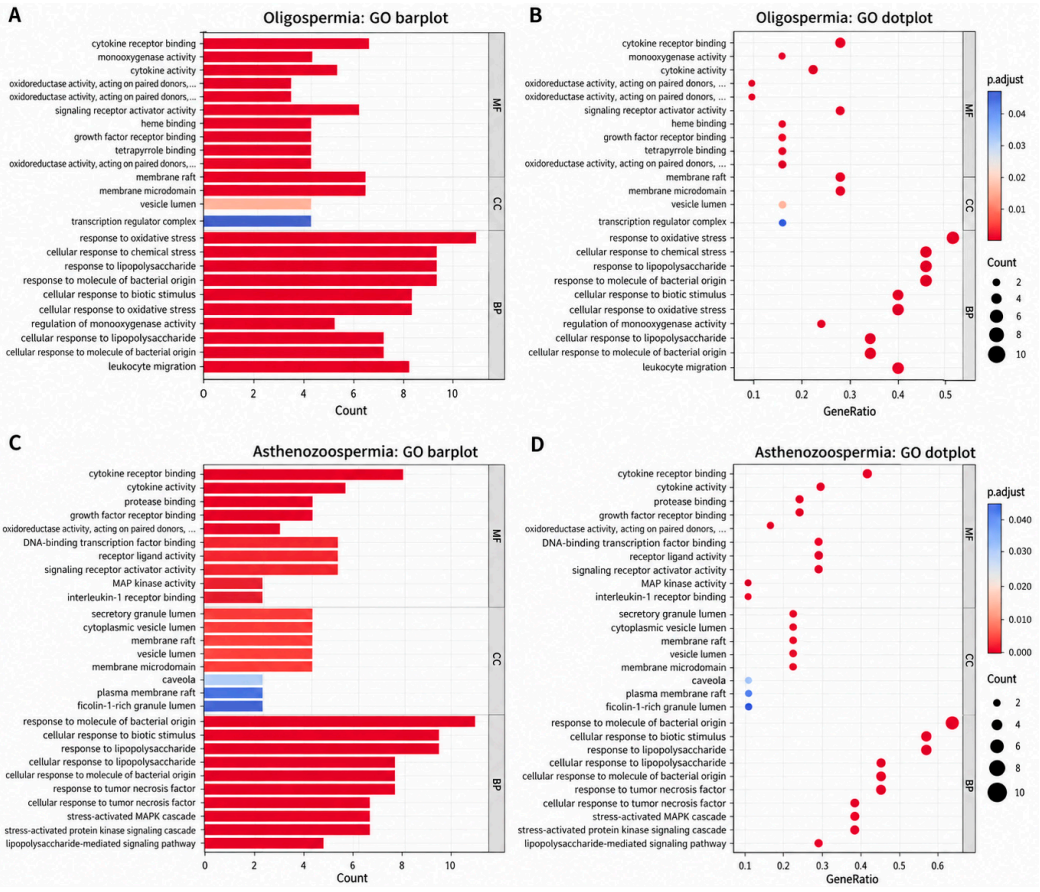


Figure 4. GO functional enrichment analysis of candidate targets for oligozoospermia and asthenozoospermia. (**A**,**B**): GO bar plot and bubble plot for oligozoospermia; (**C**,**D**): GO bar plot and bubble plot for asthenozoospermia. Color indicates the adjusted *p*-value, and bubble size indicates the number of enriched genes.

2.4. KEGG Pathway Enrichment Analysis

KEGG enrichment analysis showed that candidate targets for oligozoospermia were mainly enriched in the MAPK signaling pathway, PI3K-Akt signaling pathway, HIF-1 signaling pathway, C-type lectin receptor signaling pathway, NOD-like receptor signaling pathway, Toll-like receptor signaling pathway, TNF signaling pathway, cytosolic DNA-sensing pathway, cellular senescence, apoptosis, cytokine–cytokine receptor interaction, and sphingolipid signaling pathway (Figure 5A,B). Candidate targets for asthenozoospermia were mainly enriched in the MAPK signaling pathway, PI3K-Akt signaling pathway, TNF signaling pathway, cellular senescence, sphingolipid signaling pathway, apoptosis, HIF-1 signaling pathway, cadherin signaling, cytokine–cytokine receptor interaction, NF-kappa B signaling pathway, VEGF signaling pathway, and focal adhesion (Figure 5C,D). Several pathways, including MAPK, PI3K-Akt, TNF, HIF-1, apoptosis, and cytokine–cytokine receptor interaction, were enriched in both disease-associated target sets. The target–pathway networks further showed that these pathways were connected with highly connected candidate targets such as CXCL8, IL6, TNF, TP53, AKT1, and CASP3 (Figure 6).

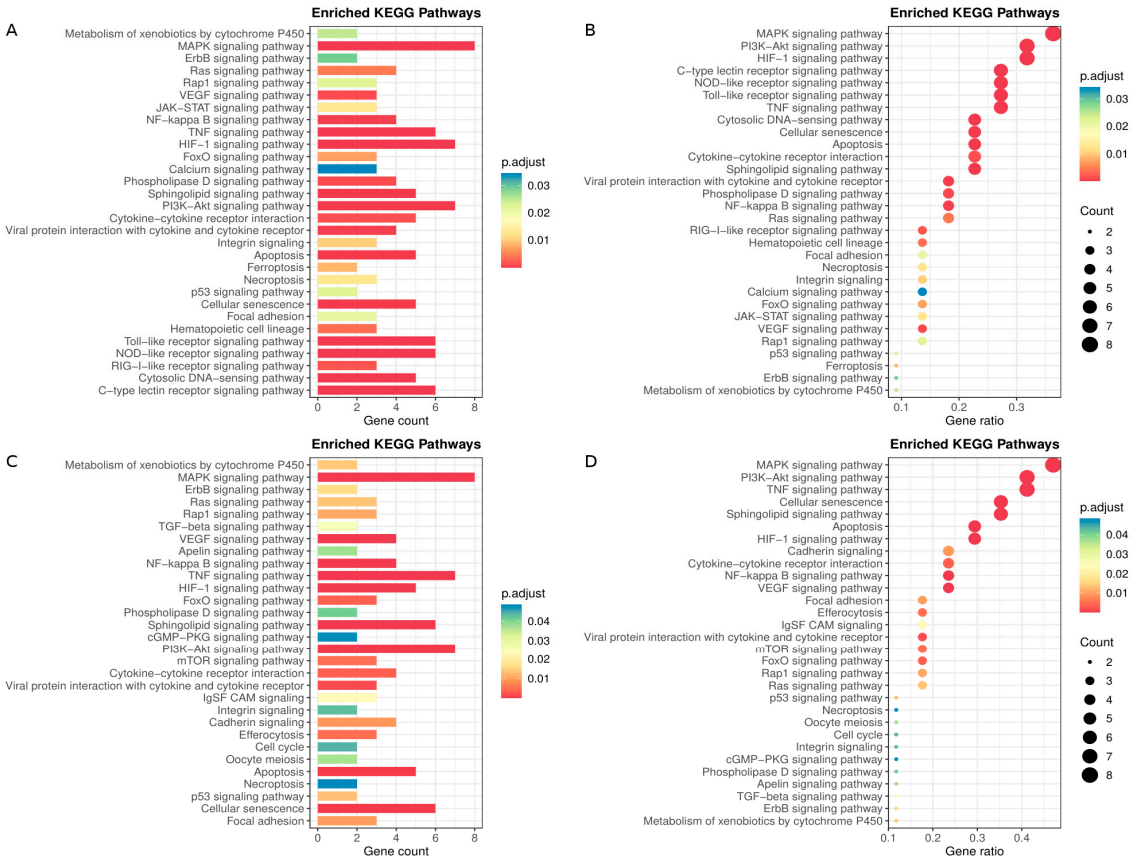


Figure 5. KEGG pathway enrichment analysis of candidate targets for oligozoospermia and asthenozoospermia. (**A**,**B**): KEGG bar plot and bubble plot for oligozoospermia; (**C**,**D**): KEGG bar plot and bubble plot for asthenozoospermia. Color indicates the adjusted *p*-value, and bubble size indicates the number of enriched genes.

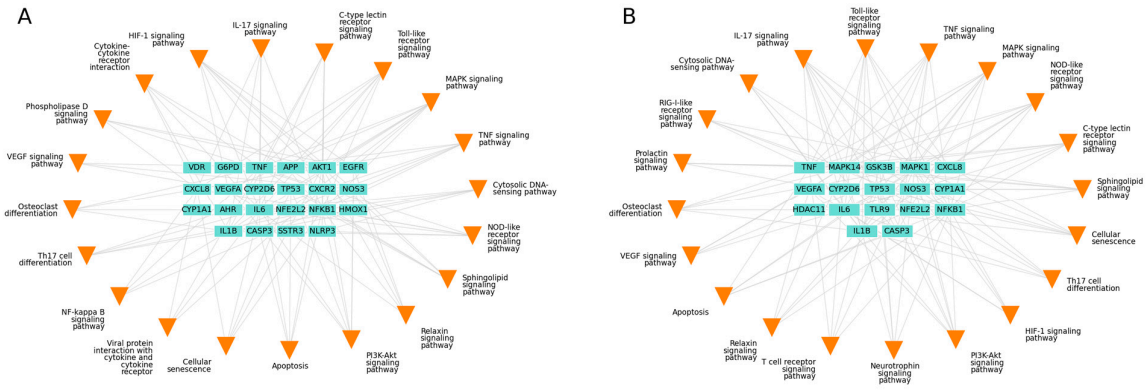


Figure 6. Target–pathway regulatory networks. (**A**): oligozoospermia target–pathway network; (**B**): asthenozoospermia target–pathway network. Blue rectangles indicate candidate targets, and orange triangles indicate significantly enriched pathways.

2.5. Physicochemical Characterization and Toxicity Prediction of Key Metabolites

SwissADME was used to characterize the physicochemical properties of the candidate metabolites. The results showed that 22 metabolites in the oligozoospermia network and 13 metabolites in the asthenozoospermia network conformed to Lipinski's rule of five. Table 2 presents eight representative metabolites from each disease network, while the physicochemical properties of all 22 and 13 metabolites satisfying Lipinski's rule of five are provided in Supplementary Table S4 for oligozoospermia and asthenozoospermia, respectively. ADMETlab-based toxicity prediction showed that most candidate metabolites did not indicate an obvious risk of hERG blockade; however, some metabolites showed positive predicted signals for human hepatotoxicity (H-HT), drug-induced liver injury (DILI), or carcinogenicity (Table 3).

Table 2. Physicochemical properties of representative metabolites associated with oligozoospermia and asthenozoospermia (eight metabolites shown for each condition). MW: molecular weight; HBA: hydrogen bond acceptors; HBD: hydrogen bond donors; MLOGP: Moriguchi octanol-water partition coefficient; TPSA: topological polar surface area.

Disease	Metabolite	MW	HBA	HBD	MLOGP	Lipinski Violations	Bioavailability Score	TPSA
Oligozoospermia	3-Phenylpropionic acid	150.17	2	1	1.98	0	0.85	37.30
Oligozoospermia	4-Hydroxyphenylacetic acid	152.15	3	2	1.05	0	0.85	57.53
Oligozoospermia	3,4-Dihydroxyphenylacetic acid	168.15	4	3	0.47	0	0.56	77.76
Oligozoospermia	Phenylacetic Acid	136.15	2	1	1.66	0	0.85	37.30
Oligozoospermia	Tryptamine	160.22	1	2	1.26	0	0.55	41.81
Oligozoospermia	2-Amino-1-methyl-6-	224.26	2	1	1.89	0	0.55	56.73

	phenylimidazo(4,5-b)pyridine							
Oligozoospermia	Capric Acid	172.26	2	1	2.58	0	0.85	37.30
Oligozoospermia	3-Indolepropionic acid	189.21	2	2	1.40	0	0.85	53.09
Asthenozoospermia	3-Phenylpropionic acid	150.17	2	1	1.98	0	0.85	37.30
Asthenozoospermia	4-Hydroxyphenylacetic acid	152.15	3	2	1.05	0	0.85	57.53
Asthenozoospermia	3,4-Dihydroxyphenylacetic acid	168.15	4	3	0.47	0	0.56	77.76
Asthenozoospermia	Phenylacetic Acid	136.15	2	1	1.66	0	0.85	37.30
Asthenozoospermia	2-Amino-1-methyl-6-phenylimidazo(4,5-b)pyridine	224.26	2	1	1.89	0	0.55	56.73
Asthenozoospermia	Capric Acid	172.26	2	1	2.58	0	0.85	37.30
Asthenozoospermia	Tyrosine	181.19	4	3	−1.70	0	0.55	83.55
Asthenozoospermia	Phenylalanine	165.19	3	2	−1.11	0	0.55	63.32

Table 3. Toxicity prediction results for key metabolites in oligozoospermia and asthenozoospermia (top eight items shown for each disease). hERG, H-HT, DILI, and carcinogenicity were classified according to ADMETlab predicted probabilities; probabilities >=0.5 were recorded as positive or blocker, and probabilities <0.5 were recorded as negative or non-blocker.

Disease	Metabolite	hERG	H-HT	DILI	Carcinogenicity	LC50DM
Oligozoospermia	3-Phenylpropionic acid	Non-blocker	negative	negative	negative	3.752
Oligozoospermia	4-Hydroxyphenylacetic acid	Non-blocker	negative	positive	negative	2.863
Oligozoospermia	3,4-Dihydroxyphenylacetic acid	Non-blocker	negative	positive	negative	3.220
Oligozoospermia	Phenylacetic Acid	Non-blocker	negative	positive	negative	3.354
Oligozoospermia	Tryptamine	Non-blocker	positive	negative	negative	4.510

Oligozoospermia	2-Amino-1-methyl-6-phenylimidazo(4,5-b)pyridine	Non-blocker	positive	positive	positive	4.502
Oligozoospermia	Capric Acid	Non-blocker	negative	negative	negative	4.766
Oligozoospermia	3-Indolepropionic acid	Non-blocker	positive	negative	negative	3.956
Asthenozoospermia	3-Phenylpropionic acid	Non-blocker	negative	negative	negative	3.752
Asthenozoospermia	4-Hydroxyphenylacetic acid	Non-blocker	negative	positive	negative	2.863
Asthenozoospermia	3,4-Dihydroxyphenylacetic acid	Non-blocker	negative	positive	negative	3.220
Asthenozoospermia	Phenylacetic Acid	Non-blocker	negative	positive	negative	3.354
Asthenozoospermia	2-Amino-1-methyl-6-phenylimidazo(4,5-b)pyridine	Non-blocker	positive	positive	positive	4.502
Asthenozoospermia	Capric Acid	Non-blocker	negative	negative	negative	4.766
Asthenozoospermia	Tyrosine	Non-blocker	positive	negative	negative	3.614
Asthenozoospermia	Phenylalanine	Non-blocker	positive	negative	negative	3.806

2.6. M-S-M-T Network Analysis

To further explore the relationships among gut microbiota, substrates, metabolites, and the prioritized candidate targets, Microbiota–Substrate–Metabolite–Target (M-S-M-T) networks were constructed. The oligozoospermia network contained 121 nodes and 158 relational edges, whereas the asthenozoospermia network contained 71 nodes and 92 relational edges (Figure 7; Supplementary Table S2). In the oligozoospermia network, AKT1 was mainly associated with metabolites such as tryptamine, 3-indolepropionic acid, indole-3-lactic acid, apigenin, luteolin, and kaempferol; CXCL8 was mainly associated with 3-phenylpropionic acid, 4-hydroxyphenylacetic acid, tyrosine, and phenylalanine; and TNF was connected to various flavonoid- or bile acid-related metabolites. In the asthenozoospermia network, CXCL8 and CASP3 were prominent connecting nodes. CXCL8 remained connected with multiple aromatic metabolites, while CASP3 was associated with metabolites such as 3-phenylpropionic acid, phenylacetic acid, and N-acetyl-L-aspartic acid. Microbial nodes such as *Bifidobacterium*, *Eubacterium ramulus*, *Clostridium sporogenes*, *Faecalibacterium prausnitzii*, *Escherichia coli*, *Akkermansia*, and *Phascolarctobacterium* were relatively prominent in the networks.

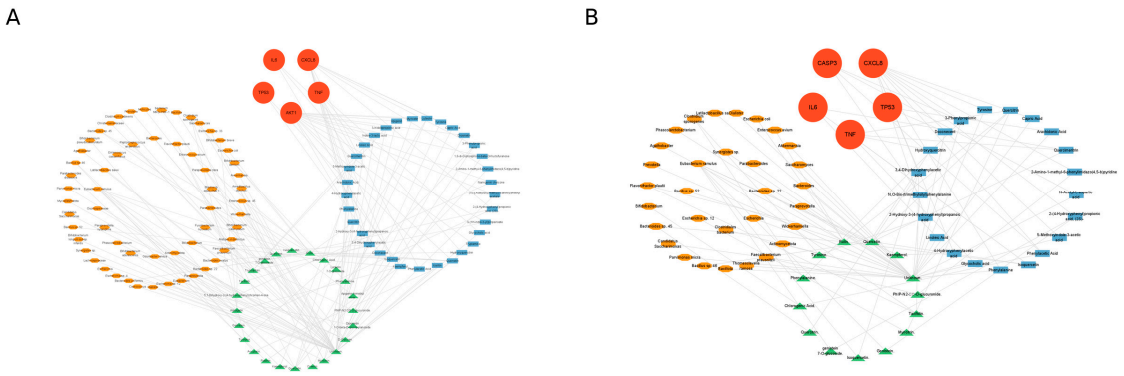


Figure 7. M-S-M-T networks. (**A**): Microbiota–Substrate–Metabolite–Target network for oligozoospermia; (**B**): Microbiota–Substrate–Metabolite–Target network for asthenozoospermia. Nodes of different colors represent gut microbiota, substrates, metabolites, and targets.

Based on the integrated microbiota–substrate–metabolite relationships and predicted metabolite–target interactions, the M-S-M-T network suggested several potential associations involving gut microbiota, aromatic metabolites, and candidate targets. Among these, a possible association involving *Clostridium sporogenes*, tyrosine/phenylalanine-derived aromatic metabolites, and CXCL8 was of particular interest, with 3-phenylpropionic acid and 4-hydroxyphenylacetic acid selected as representative metabolites for further computational analysis. Other potential associations included *Bifidobacterium*–tryptophan/indole derivatives–AKT1, *Eubacterium ramulus*–flavonoids–TNF, and phenylalanine/phenylacetic acid derivatives–CASP3 in asthenozoospermia. Together, these results highlighted aromatic metabolites and their predicted associations with CXCL8 as a common feature of the two disease networks, while other metabolite–target relationships showed differences between oligozoospermia and asthenozoospermia.

2.7. Molecular Docking Analysis

Molecular docking was performed to explore the potential interactions between two representative aromatic metabolites, 3-phenylpropionic acid and 4-hydroxyphenylacetic acid, and four shared candidate targets, CXCL8, IL6, TNF, and TP53. For CXCL8, the predicted docking scores of 3-phenylpropionic acid and 4-hydroxyphenylacetic acid were −5.6 and −5.2 kcal/mol, respectively (Table 4). LigPlot+ analysis further characterized the interactions within the predicted CXCL8 binding region. For 3-phenylpropionic acid, a predicted hydrogen bond was identified with Arg60 of chain A (2.92 Å), accompanied by nonbonded contacts involving Glu63(A/B), Lys67(A/B), Leu66(A/B), Val62(A), Glu70(B), and Gln59(A). For 4-hydroxyphenylacetic acid, predicted hydrogen bonds involved Glu63(A) and Glu70(A), with distances of 2.85 and 2.84 Å, respectively. Other nonbonded contacts involved Lys67(A/B), Gln59(B), Glu63(B), Leu66(A/B), and Val62(B) (Figure 8). The two metabolites therefore showed distinct predicted hydrogen-bonding patterns within the CXCL8 binding region.

Table 4. Molecular docking results between CXCL8 and candidate metabolites.

Protein	Metabolite	CurPocket ID	Binding Energy (kcal·mol^{-1})	Cavity Volume (Å^3)	Grid Box Centre (x, y, z)	Docking Size (x, y, z)	Main Interaction Residues
CXCL8	4-Hydroxyphenylacetic acid	C1	−5.2	324	−14, 35, 38	18, 18, 18	H-bonds: Glu63(A), Glu70(A); other contacts: Lys67(A/B), Gln59(B), Glu63(B), Leu66(A/B), Val62(B)
CXCL8	3-Phenylpropionic acid	C1	−5.6	324	−14, 35, 38	18, 18, 18	H-bond: Arg60(A); other contacts: Glu63(A/B), Lys67(A/B), Leu66(A/B), Val62(A), Glu70(B), Gln59(A)

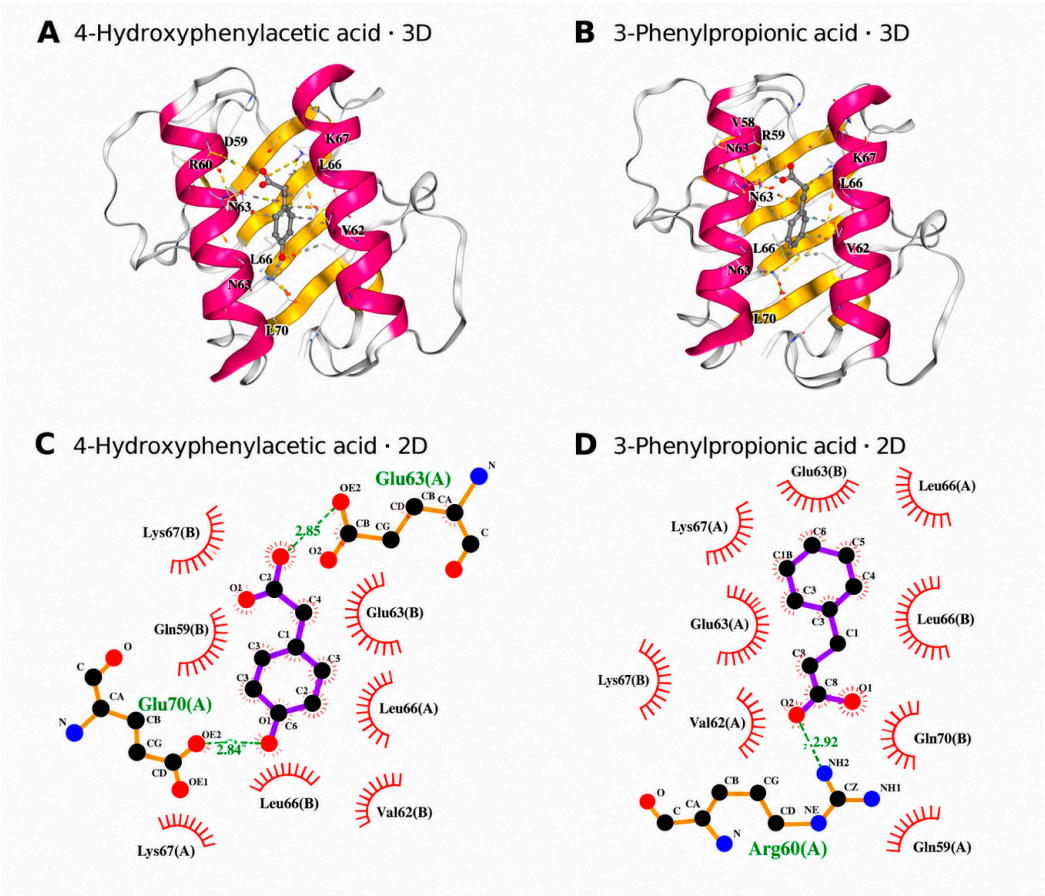


Figure 8. Three-dimensional docking poses and two-dimensional ligand–protein interaction diagrams of CXCL8 with representative aromatic metabolites. (**A**) Three-dimensional docking pose

with 4-hydroxyphenylacetic acid. (**B**) Three-dimensional docking pose with 3-phenylpropionic acid. (**C**) Two-dimensional interaction diagram with 4-hydroxyphenylacetic acid. (**D**) Two-dimensional interaction diagram with 3-phenylpropionic acid. Green dashed lines indicate predicted hydrogen bonds, and red spoked arcs indicate nonbonded contacts identified by LigPlot+.

Docking analyses were also performed for IL6, TNF, and the TP53 tetramerization domain rather than full-length TP53. The predicted scores of 3-phenylpropionic acid with these three targets were −5.1, −6.4, and −4.7 kcal/mol, respectively, while those of 4-hydroxyphenylacetic acid were −5.7, −6.5, and −4.6 kcal/mol, respectively (Supplementary Table S3).

3. Discussion

Growing evidence suggests that gut microbiota and their metabolites may be involved in male reproductive function through inflammatory and metabolic pathways [20]. In this study, we integrated microbiota–substrate–metabolite–target relationships to explore potential molecular mechanisms associated with oligozoospermia and asthenozoospermia. The identification of shared candidate targets, particularly CXCL8, IL6, TNF, and TP53, suggests that inflammatory signaling and cellular stress responses may represent common molecular features of the two conditions. These findings provide a basis for further examining how gut microbiota-derived metabolites may interact with molecular pathways relevant to sperm production and motility.

The identification of 22 candidate targets for oligozoospermia and 17 for asthenozoospermia, together with the shared highly connected targets prioritized by PPI network analysis, points to potential common involvement of inflammatory chemotaxis, cytokine signaling, and cellular stress responses in the two conditions. This result is highly consistent with previous studies on male infertility. Sperm cells are rich in polyunsaturated fatty acids and have relatively limited antioxidant systems; excessive reactive oxygen species can induce sperm membrane lipid peroxidation, decreased mitochondrial membrane potential, DNA damage, and increased apoptosis, thereby reducing sperm concentration, motility, and fertilization potential [21]. In addition, abnormal elevation of inflammatory cytokines can disrupt the local testicular and epididymal microenvironments, affecting blood–testis barrier stability, sperm maturation, and capacitation [22]. Koçak et al. found that TNF-α levels were negatively correlated with sperm motility and morphology, and that IL-6 and TNF-α were significantly correlated in seminal plasma, suggesting that both participate in the regulation of male fertility [23]. CXCL8 (interleukin-8, IL-8) is another important inflammatory mediator involved in neutrophil recruitment and local immune responses. Elevated CXCL8 levels in seminal plasma have been associated with leukocytospermia, reproductive tract inflammation, and impaired semen parameters [24–26]. A recent systematic review and meta-analysis further reported higher seminal plasma concentrations of CXCL8, IL6, and TNF in infertile men than in fertile controls [26]. Increased recruitment and activation of inflammatory cells may contribute to excessive reactive oxygen species production, potentially aggravating oxidative damage to sperm membranes and mitochondria and impairing sperm motility [7,27,28]. Together, these findings indicate that CXCL8, IL6, and TNF may be involved in the inflammatory processes associated with impaired sperm production and function, consistent with their identification as shared highly connected candidate targets in the present study.

GO enrichment results showed that the candidate targets were mainly involved in responses to molecules of bacterial origin, lipopolysaccharide responses, inflammatory responses, cytokine activity, and redox homeostasis. These findings are well corroborated by experimental studies on gut microbiota dysbiosis-induced male infertility. Ding et al.

showed that after microbiota from high-fat diet-fed mice were transplanted into normal diet-fed mice, spermatogenesis and sperm motility were impaired without significant changes in recipient body weight; these effects were accompanied by increased blood endotoxin levels, intestinal immune-cell infiltration, increased epididymal proinflammatory factors, and downregulation of genes related to testicular mitochondrial function [16]. The enrichment of responses to lipopolysaccharide and molecules of bacterial origin is consistent with the possibility that innate immune signaling, including LPS/TLR/NF-κB-related processes, may contribute to the association between gut dysbiosis and male reproductive dysfunction [29–31]. It should be noted that spermatogenesis depends on Sertoli cell support, Leydig cell endocrine function, blood–testis barrier integrity, and the epididymal maturation microenvironment [32]. Therefore, even if gut-derived inflammatory signals do not act directly on sperm, they may indirectly reduce sperm quality through systemic low-grade inflammation, local testicular immune activation, and redox imbalance.

KEGG enrichment analysis further identified MAPK, PI3K-Akt, TNF, HIF-1, NF-κB, VEGF, and other pathways among the disease-associated candidate target sets, suggesting their potential relevance to oligozoospermia and asthenozoospermia. Among them, MAPK and NF-κB are important intersections of inflammation, oxidative stress, and apoptosis [33–35]. PI3K-Akt is closely associated with Sertoli cell survival, blood–testis barrier maintenance, antioxidant responses, and spermatogenic cell proliferation [36,37]. Recent studies have shown that regulating the Src/PI3K/Akt pathway can ameliorate environmental toxicant-induced testicular injury, Cx43 abnormalities, and declines in sperm parameters [38], indicating that the PI3K-Akt pathway has protective significance in maintaining the spermatogenic microenvironment. The appearance of the HIF-1 pathway is also noteworthy. Hypoxia, inflammation, and metabolic abnormalities can activate HIF-1α, thereby affecting angiogenesis, mitochondrial metabolism, and oxidative stress levels [39]. In asthenozoospermia, mitochondrial energy supply is fundamental for maintaining flagellar movement and progressive motility. Nowicka-Bauer et al. found that decreased sperm motility in patients with asthenozoospermia is closely related to mitochondrial dysfunction and oxidative stress [40]. Hu et al. further suggested that hypoxia can increase autophagy levels and decrease motility in human sperm through the HIF-1 signaling pathway and glycolysis/gluconeogenesis pathway [41]. The co-enrichment of HIF-1, VEGF, MAPK, and TNF signaling is therefore consistent with possible links among metabolic stress, inflammatory responses, and mitochondrial function in sperm motility impairment. Considered together, these enrichment patterns may reflect a network of interrelated processes involving inflammation, cellular senescence, apoptosis, redox homeostasis, and energy metabolism in the two conditions; they do not, however, establish synergistic regulation or causal mechanisms.

The network analysis also indicated potentially different patterns of target involvement in oligozoospermia and asthenozoospermia. CXCL8, IL6, TNF, and TP53 were shared highly connected candidate nodes in both disease-associated PPI networks (Figure 9). AKT1 was among the highest-degree nodes in the oligozoospermia network, whereas CASP3 and IL1B exhibited identical topological scores across the four evaluated metrics in the asthenozoospermia network. These differences are consistent with the reported biological roles of AKT1 and CASP3 in male reproductive function. Oligozoospermia is mainly characterized by reduced sperm count and may depend more on the proliferation, survival, and differentiation of spermatogenic cells and support of the blood–testis barrier. Therefore, the prominence of AKT1 and PI3K-Akt-related cell survival signaling suggests their possible association with spermatogonial maintenance, meiotic progression, and Sertoli cell support. Kim et al. found that male mice lacking Akt1 exhibited reduced spermatogenesis, decreased sperm concentration, and impaired

fertility [42]. Lee et al. further showed that the PI3K-Akt pathway plays a key role in the self-renewing division of spermatogonial stem cells [43]. In contrast, asthenozoospermia is mainly characterized by decreased motility. The prominence of CASP3 and pathways such as apoptosis, cellular senescence, focal adhesion, cadherin signaling, and cGMP-PKG suggests that its pathological focus may involve apoptosis-like changes in mature or epididymal sperm, reduced membrane structural stability, impaired mitochondrial energy metabolism, and abnormal regulation of flagellar movement. In the study by Almeida et al., sperm caspase-3 activity was associated with asthenozoospermia and teratozoospermia [44]. Mohammadi et al. also found that low sperm motility in individuals with asthenozoospermia was associated with increased activated caspase-3 [45]. Together, these findings raise the possibility that AKT1- and CASP3-related processes may contribute differently to sperm production and motility impairment, providing a hypothesis for further investigation.

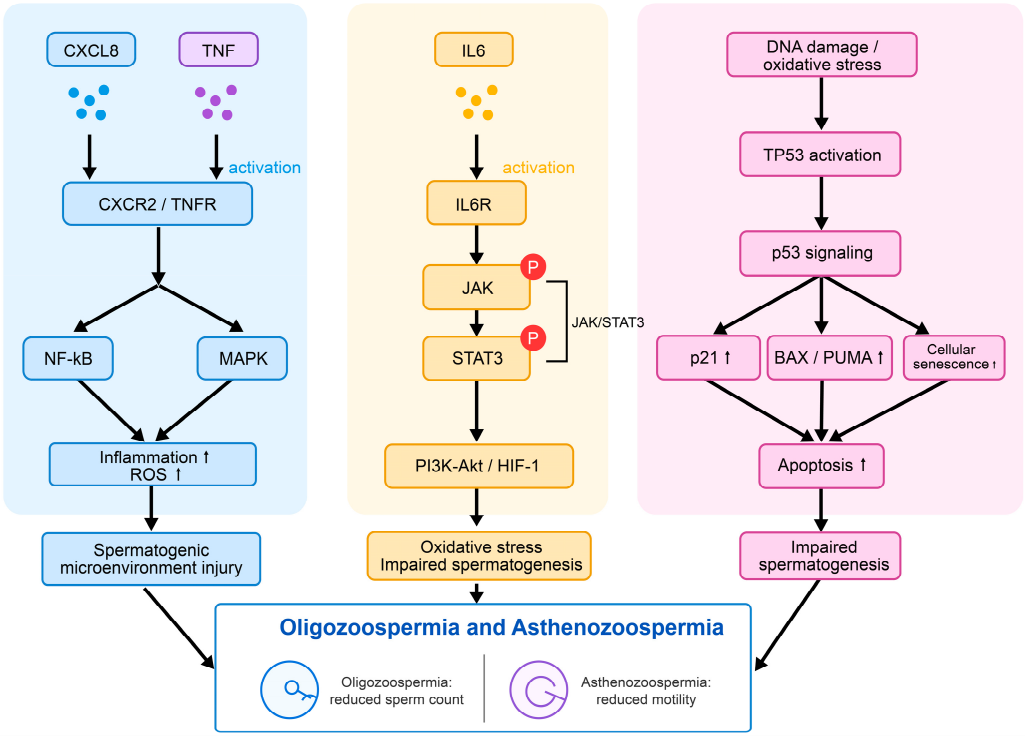


Figure 9. Schematic illustration of the potential involvement of CXCL8, TNF, IL6, and TP53 in oligozoospermia and asthenozoospermia.

The M-S-M-T network also suggested a potential association among *Clostridium sporogenes*, aromatic amino acid metabolites, and CXCL8, with 3-phenylpropionic acid and 4-hydroxyphenylacetic acid emerging as candidate metabolites of interest. This network-derived association remains hypothetical and does not establish a direct regulatory relationship between the bacterium, these metabolites, and CXCL8. Previous studies have shown that the gut microbiota can metabolize aromatic amino acids such as phenylalanine, tyrosine, and tryptophan to generate small-molecule metabolites involved in host metabolic and immune regulation [46–48]. Early work by Elsden et al. also confirmed that Clostridia can metabolize phenylalanine, tyrosine, and tryptophan and produce corresponding end products [49]. These studies support the involvement of *Clostridium* species in aromatic amino acid metabolism and provide a biological context for the candidate relationships identified in our network analysis. It should be emphasized that the biological effects of aromatic metabolites may be context dependent.

Wu et al. found that 4-hydroxyphenylacetic acid can exert protective effects by regulating intestinal inflammation or metabolic pathways [50]. Wang et al. also showed that resveratrol supplementation can improve high-fat diet-related obesity, glucose and lipid metabolic disorders, and systemic inflammation through the gut microbiota-derived 4-hydroxyphenylacetic acid-SIRT1 axis [51]. Conversely, a study by Wang et al. on atherosclerosis suggested that *Desulfovibrio piger* can convert phenylalanine into 3-phenylpropionic acid, which serves as a precursor of hippuric acid in the phenylalanine metabolic axis, while hippuric acid can promote atherosclerosis progression and increase inflammatory cytokine secretion [52]. The potential interactions of 3-phenylpropionic acid and 4-hydroxyphenylacetic acid with CXCL8 may be relevant to inflammatory signaling, although their biological effects are likely to depend on metabolite concentration, tissue context, and host metabolic status. Further studies are needed to explore whether these metabolites can influence CXCL8-related responses in the male reproductive system. As CXCL8 plays a central role in inflammatory cell recruitment, changes in CXCL8-related signaling could potentially affect the local inflammatory environment of the male reproductive tract. However, whether these aromatic metabolites directly regulate CXCL8 expression or activity remains to be determined.

Molecular docking analysis yielded predicted binding energies of −5.6 kcal/mol and −5.2 kcal/mol for 3-phenylpropionic acid and 4-hydroxyphenylacetic acid with CXCL8, respectively [53]. The slightly more favorable docking score of 3-phenylpropionic acid suggests that it may be a candidate for further investigation, although the predicted scores alone do not determine actual binding affinity or biological activity. As re-docking validation and RMSD assessment were not performed due to the lack of suitable co-crystallized reference ligands, these results should be regarded solely as exploratory computational predictions rather than evidence of direct molecular binding. Although both metabolites yielded more negative docking scores with TNF (−6.4 and −6.5 kcal/mol, respectively), these scores should not be interpreted as evidence of greater biological relevance, particularly when comparing predictions across different receptor structures. Both 3-phenylpropionic acid and 4-hydroxyphenylacetic acid met Lipinski's rule of five [54], while ADMETlab predicted potential toxicity signals for some aromatic metabolites. These results provide supplementary information on the properties of the candidate metabolites, whose biological effects and safety warrant further investigation under physiologically relevant conditions. Future studies could use surface plasmon resonance (SPR) or microscale thermophoresis (MST) to assess potential binding between these metabolites and CXCL8, with cellular thermal shift assays (CETSA) providing complementary evidence where appropriate. Functional studies using Sertoli cells, spermatogenic cells, epididymal epithelial cells, or spermatozoa may further explore their effects on CXCL8-related inflammatory responses, oxidative stress, mitochondrial function, and sperm motility.

Dietary interventions may also be relevant to the potential relationships among gut microbiota, microbial metabolites, and CXCL8 suggested by our network analysis. Diet can alter gut microbial composition and metabolic activity, potentially influencing the production of microbial metabolites, including those derived from aromatic amino acids [55]. Previous dietary intervention studies have shown that changes in gut microbial composition and function can be accompanied by changes in immune and inflammatory responses [56]. Moreover, studies on personalized nutrition have demonstrated considerable interindividual variability in metabolic responses to dietary intake, with gut microbiota profiles contributing to these differences [57,58]. The potential relationships among diet, gut microbiota composition, and aromatic metabolites may therefore be relevant to future studies of inflammatory regulation in male reproductive health. However, whether such interventions can directly affect CXCL8 expression or activity and

improve sperm quality in men with oligozoospermia or asthenozoospermia remains unclear. For clinical translation, future studies could combine gut microbiota profiling and targeted metabolomics with measurements of seminal CXCL8, inflammatory markers, and conventional semen parameters. These analyses could help characterize patient-specific microbial and metabolic patterns and examine their associations with reproductive outcomes. Further experimental studies and prospective dietary interventions are needed to evaluate the biological effects of the identified metabolites on CXCL8 and determine whether microbiota-targeted nutritional strategies can improve male reproductive health.

This study has several limitations. First, the analysis mainly relies on public databases, target prediction, PPI topology, and molecular docking, and the proposed metabolite–target relationships require further experimental investigation. The results may also be influenced by differences in database coverage and the predictive performance of computational methods. The use of gutMGene host genes as an additional filter may introduce literature coverage bias by preferentially retaining previously documented microbiota-associated host genes. Although CXCL8, IL6, TNF, and TP53 remained among the candidate targets when the gutMGene filter was omitted, the database-specific sensitivity analysis revealed that their retention varied under alternative prediction and disease-gene filtering criteria. In particular, stricter GeneCards Relevance Score thresholds substantially reduced the candidate target sets. These findings indicate that target prioritization depends on methodological choices and should be interpreted accordingly. In addition, the relatively small size of the PPI networks and the use of an operational top-ranking cutoff may influence candidate node prioritization, even when complementary topological metrics are considered. Further evaluation using additional topological measures and network stability analyses would help assess the robustness of these findings. Furthermore, the identified metabolites have not been measured in patient samples, and their potential effects on CXCL8 expression or activity remain to be examined experimentally. Second, the M-S-M-T network integrates microbiota–substrate–metabolite relationships from gutMGene with computationally predicted metabolite–target interactions. As these relationships are derived from studies with different experimental settings and levels of evidence, they may not fully reflect the actual microbial metabolic activity or host responses in patients with oligozoospermia and asthenozoospermia. Third, semen quality is affected by multiple factors, including age, BMI, diet, smoking and alcohol consumption, abstinence duration, infection, varicocele, and environmental exposure; database analyses cannot adequately adjust for these confounders. Independent clinical cohorts with detailed participant information are needed to evaluate the clinical relevance of the predicted associations. Fourth, molecular docking was performed using the default parameters of the CB-Dock2 server. Because suitable co-crystallized small-molecule reference ligands were unavailable for the selected protein structures, re-docking validation and RMSD assessment were not performed. Consequently, the docking results should be interpreted solely as exploratory computational predictions, rather than as validated evidence of molecular binding. The structural characteristics of the selected protein models and the moderate docking scores should also be considered when interpreting these findings. Their physiological relevance depends on whether these metabolites reach biologically relevant concentrations in the testis, epididymis, or seminal microenvironment and influence CXCL8-related responses. Future studies integrating 16S rRNA sequencing or metagenomics, targeted metabolomics, and transcriptomics may help evaluate the predicted associations among gut microbiota, microbial metabolites, host targets, and male reproductive function, and provide a basis for exploring potential microbiota-targeted interventions.

4. Materials and Methods

4.1. Acquisition of Gut Microbiota Metabolites and Their Potential Targets

Information on gut microbiota, substrates, metabolites, and corresponding host genes was retrieved from gutMGene v2.0 (http://bio-computing.hrbmu.edu.cn/gutmgene; accessed on 4 June 2026) [59]. The initial dataset contained 2488 records, involving 446 distinct microbial names, 161 distinct nonempty substrate names, and 614 distinct metabolite names. After restricting the dataset to human-associated records, 830 records involving 260 microbial names, 125 nonempty substrate names, and 251 metabolite names were retained. Metabolites were matched to PubChem to obtain compound identifiers and SMILES representations. Following structural matching and the exclusion of compounds with SMILES strings exceeding 200 characters, 784 records involving 226 distinct metabolites were retained. Detailed screening criteria and stage-specific counts are provided in Supplementary Table S5.

The SMILES strings were submitted to SwissTargetPrediction (https://www.swisstargetprediction.ch/, accessed on 4 June 2026) and the Similarity Ensemble Approach (SEA; https://sea.bkslab.org/), accessed on 4 June 2026. For SwissTargetPrediction, predictions with a probability greater than 0.1 were retained. For SEA, only predictions annotated as human targets were retained, without applying an additional *p*-value cutoff. Database-specific filtering criteria were adopted to account for differences in the prediction methodologies and scoring systems of SwissTargetPrediction and SEA. Gene symbols were extracted from the retained predictions, and entries containing multiple symbols were separated. The target lists from both databases were merged and deduplicated to obtain the predicted metabolite-related target set. A Venn diagram was used to illustrate the overlap between the two prediction sets. The filtering procedures and target counts for individual metabolites are detailed in Supplementary Table S5.

4.2. Screening of Disease Targets for Oligozoospermia and Asthenozoospermia

Disease-related targets were retrieved from GeneCards (v5.26), Online Mendelian Inheritance in Man (OMIM) [60], and the Comparative Toxicogenomics Database (CTD) [61] on 4 June 2026, using "oligozoospermia" and "asthenozoospermia" as disease-specific search terms, with "oligospermia" included as an additional retrieval term to capture records indexed under this alternative terminology. In GeneCards, protein-coding genes with a Relevance Score greater than 1 were retained. OMIM records were retrieved using Gene Map Search, whereas CTD records were restricted to curated disease–gene associations. Gene symbols were compiled separately for each disease and deduplicated during integration. Detailed database-specific retrieval and filtering criteria are provided in Supplementary Table S5. The predicted metabolite targets, disease-related targets, and human host genes from gutMGene were further intersected to identify candidate targets potentially associated with oligozoospermia and asthenozoospermia. The gutMGene host gene filter was used to prioritize candidate targets with previously documented microbiota- or metabolite-associated host gene relationships [59,62]. Because this approach may introduce literature coverage bias, we additionally compared the candidate target sets obtained with and without this filter. Specifically, the two-source intersection of predicted metabolite targets and disease-associated genes was compared with the original three-source intersection that also included gutMGene human host genes. All other screening criteria remained unchanged. The detailed comparison is provided in Supplementary Table S7. Gut–Target–Oligozoospermia and Gut–Target–Asthenozoospermia regulatory networks were constructed using Cytoscape 3.9.0.

To assess the sensitivity of candidate target selection to database-specific filtering criteria, alternative SwissTargetPrediction probability thresholds (>0.2 and >0.3), SEA *p*-value thresholds (≤1×10^{-5} and ≤1×10^{-10}), and GeneCards Relevance Score thresholds (>1.5 and >2) were evaluated individually, with the other screening criteria unchanged. Candidate target sets were recalculated separately for oligozoospermia and asthenozoospermia and compared with the original sets using the Jaccard similarity index. Detailed results are presented in Supplementary Table S6.

4.3. PPI Network Construction and Candidate Target Prioritization

Candidate targets for oligozoospermia and asthenozoospermia were imported separately into the STRING database (https://string-db.org/), with the species set to Homo sapiens and the minimum required interaction score set to 0.400 (medium confidence). Protein–protein interaction (PPI) networks were constructed using the candidate targets without adding additional interacting proteins. All nodes in the resulting networks had at least one interaction, with no isolated nodes present. Network data were imported into Cytoscape for visualization and topological analysis. Degree centrality (DC) was used as the primary criterion for prioritizing highly connected nodes in each PPI network. The five highest-ranked nodes were initially selected as a prioritization set [63,64]. When nodes had identical DC values at the selection boundary, all tied nodes were retained to avoid arbitrary exclusion. Betweenness centrality (BC), closeness centrality (CC), and maximal clique centrality (MCC) were additionally calculated to characterize complementary aspects of network topology and compare the rankings obtained using different metrics. Shared highly connected candidate targets of oligozoospermia and asthenozoospermia were then identified by intersection analysis. Node size and color intensity in the network were mapped according to DC values to reflect the relative importance of each target.

4.4. GO Functional and KEGG Pathway Enrichment Analyses

Gene Ontology (GO) functional enrichment and Kyoto Encyclopedia of Genes and Genomes (KEGG) pathway enrichment analyses were performed for candidate targets of the two diseases using the "clusterProfiler" and "org.Hs.eg.db" packages in R. GO analysis included three categories: biological process (BP), cellular component (CC), and molecular function (MF). In KEGG analysis, the species parameter was set to human, and the Benjamini–Hochberg method was used for multiple testing correction. An adjusted *p*-value < 0.05 was considered statistically significant. Major enriched terms were selected according to gene count, gene ratio, and adjusted *p*-value and visualized using bar plots and bubble plots. Significantly enriched pathways and their related targets were further extracted and imported into Cytoscape to construct target–pathway regulatory networks.

4.5. Physicochemical Characterization and Toxicity Prediction of Key Metabolites

Candidate metabolites associated with highly connected candidate targets were identified based on metabolite–target relationships, and their physicochemical properties were characterized using SwissADME. The main parameters assessed included molecular weight (MW), number of hydrogen bond acceptors (HBA), number of hydrogen bond donors (HBD), Moriguchi octanol-water partition coefficient (MLOGP), topological polar surface area (TPSA), number of Lipinski rule violations, and bioavailability score. Metabolites satisfying MW < 500, MLOGP < 5, HBA < 10, HBD ≤ 5, and TPSA < 140 $Å^2$, with no Lipinski rule violations, were recorded as meeting these physicochemical criteria for descriptive purposes only, without implying pharmacological suitability, safety, or therapeutic potential.

ADMETlab was used to predict the toxicity of candidate metabolites. The evaluated indicators included the risk of human ether-à-go-go-related gene potassium channel blockade (hERG), human hepatotoxicity (H-HT), drug-induced liver injury (DILI), carcinogenicity, and the rat acute toxicity index LC50DM. For hERG, H-HT, DILI, and carcinogenicity, a predicted probability ≥ 0.5 was defined as positive or blocker, whereas a predicted probability < 0.5 was defined as negative or non-blocker.

4.6. Construction of M-S-M-T Networks

To explore potential relationships among gut microbiota, substrates, metabolites, and candidate targets associated with oligozoospermia and asthenozoospermia, microbiota–substrate and substrate–metabolite relationships from the gutMGene database were integrated with metabolite target prediction results and PPI-based candidate target prioritization results. Microbiota–Substrate–Metabolite–Target (M-S-M-T) networks were established separately for oligozoospermia and asthenozoospermia. Network relationship files and node attribute files were organized and imported into Cytoscape for visualization. Different colors and shapes represented gut microbiota, substrates, metabolites, and targets, and node size was adjusted according to network degree. The network was further examined to identify highly connected nodes and potential microbiota–substrate–metabolite–target associations for future investigation.

4.7. Molecular Docking Analysis

Based on the PPI and M-S-M-T network analyses, CXCL8, IL6, TNF, and TP53 were selected for molecular docking with 3-phenylpropionic acid and 4-hydroxyphenylacetic acid. Among the shared highly connected candidate targets, CXCL8 was selected for more detailed docking analysis based on its high connectivity in both disease-associated PPI networks and its predicted links to both representative aromatic metabolites in the M-S-M-T network. The three-dimensional structures of 3-phenylpropionic acid and 4-hydroxyphenylacetic acid were obtained from PubChem in SDF format. Protein structures were retrieved from the RCSB Protein Data Bank, including CXCL8 (PDB ID: 1ICW; dimeric model, chains A and B; resolution: 2.01 Å), IL6 (PDB ID: 1ALU; single-chain model, chain A; resolution: 1.90 Å), TNF (PDB ID: 1A8M; trimeric model, chains A–C; resolution: 2.30 Å), and the TP53 tetramerization domain (PDB ID: 1AIE; single-chain fragment, chain A, residues 326–356; resolution: 1.50 Å).

Molecular docking was performed using the cavity detection-guided docking workflow of the CB-Dock2 online server, which integrates automated binding-site identification with AutoDock Vina (version 1.2.0) [65]. According to the server workflow, protein preparation includes the addition of missing side-chain atoms and hydrogen atoms and the removal of crystallographic water molecules and other hetero groups, while ligand preparation includes hydrogen addition, partial charge assignment, and three-dimensional structure processing using RDKit. For each predicted cavity, CB-Dock2 automatically defines a localized docking search region based on the cavity geometry, with docking performed using the default parameters of the CB-Dock2 server. For CXCL8, the selected C1 cavity had a volume of 324 $Å^3$, with a server-generated docking box centered at (−14, 35, 38) Å and measuring 18 × 18 × 18 Å (Table 4). The predicted binding poses were ranked according to their docking scores, with more negative Vina scores indicating more favorable predicted interactions within the scoring model. The docking poses and surrounding contact residues were examined using the server's interactive NGL Viewer. Two-dimensional ligand–protein interaction diagrams for the selected CXCL8 complexes were generated using LigPlot+ (version 2.2.9) to identify predicted hydrogen bonds and nonbonded contacts [66]. Re-docking validation and root-mean-

square deviation (RMSD) assessment were not performed because suitable co-crystallized small-molecule reference ligands were unavailable for the selected protein structures.

5. Conclusions

This study systematically explored the potential associations between gut microbiota-derived metabolites and oligozoospermia and asthenozoospermia using a network pharmacology approach. The analysis identified CXCL8, IL6, TNF, and TP53 as shared highly connected candidate targets of the two conditions. Enrichment of pathways involving MAPK, PI3K-Akt, TNF, HIF-1, NF-κB, and apoptosis may reflect biological processes associated with impaired spermatogenesis and reduced sperm motility. The M-S-M-T network further suggested a potential association involving *Clostridium sporogenes*, tyrosine/phenylalanine-derived aromatic metabolites, and CXCL8, providing a hypothesis for further experimental investigation. Molecular docking predicted possible interactions of 3-phenylpropionic acid and 4-hydroxyphenylacetic acid with CXCL8, providing computational hypotheses for subsequent testing. These findings provide a basis for further investigation of potential relationships among gut microbiota, metabolites, and male reproductive function, particularly through experimental and clinical validation of the identified candidate targets and metabolic associations.

Supplementary Materials: The following supporting information can be downloaded at: https://www.mdpi.com/article/10.3390/ijms272210384/s1.

Author Contributions: Q.S. and Y.B. conceived and designed the study. W.F. collected and curated the data. Q.S. performed target prediction, network construction, enrichment analysis, drug-likeness and toxicity evaluation, and molecular docking. J.W. and K.W. prepared the figures and tables. K.W. and Q.S. drafted the manuscript. J.W. critically revised the manuscript for important intellectual content. All authors have read and agreed to the published version of the manuscript.

Funding: This research received no external funding.

Institutional Review Board Statement: Not applicable. This study was based on publicly available databases and in silico analyses, and did not involve human participants, human data, human tissue, animals, or any clinical intervention.

Informed Consent Statement: Not applicable. This manuscript does not contain any individual person's data in any form.

Data Availability Statement: All data generated or analysed during this study are included in this published article and its supplementary information files.

Conflicts of Interest: The authors declare that they have no competing interests.

References

1. Eisenberg, M.L.; Esteves, S.C.; Lamb, D.J.; Hotaling, J.M.; Giwercman, A.; Hwang, K.; Cheng, Y.S. Male infertility. *Nat. Rev. Dis. Primers* **2023**, *9*, 49. https://doi.org/10.1038/s41572-023-00459-w.
2. Leslie, S.W.; Soon-Sutton, T.L.; Khan, M.A.B. Male Infertility. In *StatPearls*; StatPearls Publishing: Treasure Island, FL, USA, 2026.
3. Björndahl, L.; Kirkman Brown, J.; WHO Laboratory Manual Editorial Board Members. The sixth edition of the WHO Laboratory Manual for the Examination and Processing of Human Semen: Ensuring quality and standardization in basic examination of human ejaculates. *Fertil. Steril.* **2022**, *117*, 246–251. https://doi.org/10.1016/j.fertnstert.2021.12.012.
4. Stormont, G.D.; Deibert, C.M. Genetic causes and management of male infertility. *Transl. Androl. Urol.* **2021**, *10*, 1365–1372. https://doi.org/10.21037/tau.2020.03.34.
5. Babakhanzadeh, E.; Nazari, M.; Ghasemifar, S.; Khodadadian, A. Some of the Factors Involved in Male Infertility: A Prospective Review. *Int. J. Gen. Med.* **2020**, *13*, 29–41. https://doi.org/10.2147/IJGM.S241099.

6. Bao, B.; Wen, H.; Wang, F.; Han, D.; Liu, B. Inflammation of the male reproductive system: Clinical aspects and mechanisms. *Front. Endocrinol.* **2025**, *16*, 1547020. Correction in *Front. Endocrinol.* **2025**, *16*, 1649509. https://doi.org/10.3389/fendo.2025.1547020.
7. Takeshima, T.; Usui, K.; Mori, K.; Asai, T.; Yasuda, K.; Kuroda, S.; Yumura, Y. Oxidative stress and male infertility. *Reprod. Med. Biol.* **2021**, *20*, 41–52. https://doi.org/10.1002/rmb2.12353.
8. Wang, Y.; Fu, X.; Li, H. Mechanisms of oxidative stress-induced sperm dysfunction. *Front. Endocrinol.* **2025**, *16*, 1520835. https://doi.org/10.3389/fendo.2025.1520835.
9. Pérez, C.V.; Sobarzo, C.M.; Jacobo, P.V.; Pellizzari, E.H.; Cigorraga, S.B.; Denduchis, B.; Lustig, L. Loss of occludin expression and impairment of blood-testis barrier permeability in rats with autoimmune orchitis: Effect of interleukin 6 on Sertoli cell tight junctions. *Biol. Reprod.* **2012**, *87*, 122.
10. Fan, Y.; Pedersen, O. Gut microbiota in human metabolic health and disease. *Nat. Rev. Microbiol.* **2021**, *19*, 55–71. https://doi.org/10.1038/s41579-020-0433-9.
11. Hey, G.E.; Vedam-Mai, V.; Beke, M.; Amaris, M.; Ramirez-Zamora, A. The Interface between Inflammatory Bowel Disease, Neuroinflammation, and Neurological Disorders. *Semin. Neurol.* **2023**, *43*, 572–582. https://doi.org/10.1055/s-0043-1771467.
12. Cai, H.; Cao, X.; Qin, D.; Liu, Y.; Liu, Y.; Hua, J.; Peng, S. Gut microbiota supports male reproduction via nutrition, immunity, and signaling. *Front. Microbiol.* **2022**, *13*, 977574. https://doi.org/10.3389/fmicb.2022.977574.
13. Magill, R.G.; MacDonald, S.M. Male infertility and the human microbiome. *Front. Reprod. Health.* **2023**, *5*, 1166201. https://doi.org/10.3389/frph.2023.1166201.
14. Lundy, S.D.; Sangwan, N.; Parekh, N.V.; Selvam, M.K.P.; Gupta, S.; McCaffrey, P.; Bessoff, K.; Vala, A.; Agarwal, A.; Sabanegh, E.S.; et al. Functional and Taxonomic Dysbiosis of the Gut, Urine, and Semen Microbiomes in Male Infertility. *Eur. Urol.* **2021**, *79*, 826–836. https://doi.org/10.1016/j.eururo.2021.01.014.
15. Pan, Y.; Wang, S.; Liu, L.; Liu, X. Characteristics of gut microbiota in patients with asthenozoospermia: A Chinese pilot study. *BMC Microbiol.* **2024**, *24*, 22. https://doi.org/10.1186/s12866-023-03173-5.
16. Ding, N.; Zhang, X.; Zhang, X.D.; Jing, J.; Liu, S.S.; Mu, Y.P.; Peng, L.L.; Yan, Y.J.; Xiao, G.M.; Bi, X.Y.; et al. Impairment of spermatogenesis and sperm motility by the high-fat diet-induced dysbiosis of gut microbes. *Gut* **2020**, *69*, 1608–1619. https://doi.org/10.1136/gutjnl-2019-319127.
17. Hao, Y.; Feng, Y.; Yan, X.; Chen, L.; Zhong, R.; Tang, X.; Shen, W.; Sun, Q.; Sun, Z.; Ren, Y.; et al. Gut microbiota-testis axis: FMT improves systemic and testicular micro-environment to increase semen quality in type 1 diabetes. *Mol. Med.* **2022**, *28*, 45. https://doi.org/10.1186/s10020-022-00473-w.
18. Hao, Y.; Feng, Y.; Yan, X.; Chen, L.; Ma, X.; Tang, X.; Zhong, R.; Sun, Z.; Agarwal, M.; Zhang, H.; et al. Gut Microbiota-Testis Axis: FMT Mitigates High-Fat Diet-Diminished Male Fertility via Improving Systemic and Testicular Metabolome. *Microbiol. Spectr.* **2022**, *10*, e0002822. https://doi.org/10.1128/spectrum.00028-22.
19. Nogales, C.; Mamdouh, Z.M.; List, M.; Kiel, C.; Casas, A.I.; Schmidt, H.H.H.W. Network pharmacology: Curing causal mechanisms instead of treating symptoms. *Trends Pharmacol. Sci.* **2022**, *43*, 136–150.
20. Pan, M.; O'Flaherty, C. Gut Microbial Dysbiosis and Male Reproductive Health: Current Insights and Future Directions. *Int. J. Mol. Sci.* **2026**, *27*, 4482. https://doi.org/10.3390/ijms27104482.
21. Kurhaluk, N.; Kamiński, P.; Tkaczenko, H. Oxidative Stress, Antioxidants, Gut Microbiota and Male Fertility. *Cell. Physiol. Biochem.* **2025**, *59*, 82–123. https://doi.org/10.33594/000000802.
22. Fomichova, O.; Oliveira, P.F.; Bernardino, R.L. Exploring the interplay between inflammation and male fertility. *FEBS J.* **2025**, *292*, 3321–3349. https://doi.org/10.1111/febs.17366.
23. Koçak, I.; Yenisey, C.; Dündar, M.; Okyay, P.; Serter, M. Relationship between seminal plasma interleukin-6 and tumor necrosis factor alpha levels with semen parameters in fertile and infertile men. *Urol. Res.* **2002**, *30*, 263–267. https://doi.org/10.1007/s00240-002-0269-y.
24. Maegawa, M.; Kamada, M.; Irahara, M.; Yamamoto, S.; Yoshikawa, S.; Kasai, Y.; Ohmoto, Y.; Gima, H.; Thaler, C.J.; Aono, T. A repertoire of cytokines in human seminal plasma. *J. Reprod. Immunol.* **2002**, *54*, 33–42. https://doi.org/10.1016/s0165-0378(01)00063-8.
25. Saxena, P.; Soni, R.; Randhawa, V.S.; Singh, N. Can Seminal IL-8 Level Be Used as a Marker of Leukocytospermia and Does It Have Any Correlation with Semen Parameters in Infertile Couples? *J. Obstet. Gynaecol. India* **2019**, *69*, 451–456.
26. Lyons, H.E.; Arriaran Scott, C.N.; Robertson, S.A.; Sharkey, D.J. Seminal plasma cytokines in fertile versus infertile men: A systematic review and meta-analysis. Hum. *Reprod. Update* **2026**, *32*, 381–408. https://doi.org/10.1093/humupd/dmag003.

27. Pavuluri, H.; Bakhtiary, Z.; Selvam, M.K.P.; Hellstrom, W.J.G. Oxidative Stress-Associated Male Infertility: Current Diagnostic and Therapeutic Approaches. *Medicina* **2024**, *60*, 1008. https://doi.org/10.3390/medicina60061008.
28. Nowicka-Bauer, K.; Nixon, B. Molecular Changes Induced by Oxidative Stress that Impair Human Sperm Motility. *Antioxidants* **2020**, *9*, 134. https://doi.org/10.3390/antiox9020134.
29. Hedger, M.P. Toll-like receptors and signalling in spermatogenesis and testicular responses to inflammation--a perspective. *J. Reprod. Immunol.* **2011**, *88*, 130–141.
30. Sahnoun, S.; Sellami, A.; Chakroun, N.; Mseddi, M.; Attia, H.; Rebai, T.; Lassoued, S. Human sperm Toll-like receptor 4 (TLR4) mediates acrosome reaction, oxidative stress markers, and sperm parameters in response to bacterial lipopolysaccharide in infertile men. *J. Assist. Reprod. Genet.* **2017**, *34*, 1067–1077.
31. Pan, Y.; Liu, Y.; Wang, L.; Xue, F.; Hu, Y.; Hu, R.; Xu, C. MKP-1 attenuates LPS-induced blood-testis barrier dysfunction and inflammatory response through p38 and IκBα pathways. *Oncotarget* **2016**, *7*, 84907–84923. https://doi.org/10.18632/oncotarget.12823.
32. O'Donnell, L.; Smith, L.B.; Rebourcet, D. Sertoli cells as key drivers of testis function. *Semin. Cell. Dev. Biol.* **2022**, *121*, 2–9. https://doi.org/10.1016/j.semcdb.2021.06.016.
33. Dutta, S.; Sengupta, P.; Slama, P.; Roychoudhury, S. Oxidative Stress, Testicular Inflammatory Pathways, and Male Reproduction. *Int. J. Mol. Sci.* **2021**, *22*, 10043. https://doi.org/10.3390/ijms221810043.
34. Kumar, L.; Solanki, S.; Jain, A.; Botts, M.; Gupta, R.; Rajput, S.; Roti Roti, E. MAPKs signaling is obligatory for male reproductive function in a development-specific manner. *Front. Reprod. Health.* **2024**, *6*, 1330161.
35. Pentikäinen, V.; Suomalainen, L.; Erkkilä, K.; Martelin, E.; Parvinen, M.; Pentikäinen, M.O.; Dunkel, L. Nuclear factor-kappa B activation in human testicular apoptosis. *Am. J. Pathol.* **2002**, *160*, 205–218.
36. Chen, K.Q.; Wei, B.H.; Hao, S.L.; Yang, W.X. The PI3K/AKT signaling pathway: How does it regulate development of Sertoli cells and spermatogenic cells? *Histol. Histopathol.* **2022**, *37*, 621–636.
37. Wanjari, U.R.; Gopalakrishnan, A.V. Blood-testis barrier: A review on regulators in maintaining cell junction integrity between Sertoli cells. *Cell Tissue Res.* **2024**, *396*, 157–175. https://doi.org/10.1007/s00441-024-03894-7.
38. Li, H.; Wang, H.; Xu, X.; Qu, L.; Sun, X.; Zhang, J. Protective effect of ginsenoside Rg3 on DBP-induced spermatogenesis injury via the Src/PI3K signaling pathway. *Reprod. Toxicol.* **2025**, *138*, 109047.
39. Semenza, G.L. Hypoxia-inducible factor 1: Regulator of mitochondrial metabolism and mediator of ischemic preconditioning. *Biochim. Biophys. Acta.* **2011**, *1813*, 1263–1268.
40. Nowicka-Bauer, K.; Lepczynski, A.; Ozgo, M.; Kamieniczna, M.; Fraczek, M.; Stanski, L.; Olszewska, M.; Malcher, A.; Skrzypczak, W.; Kurpisz, M.K. Sperm mitochondrial dysfunction and oxidative stress as possible reasons for isolated asthenozoospermia. *J. Physiol. Pharmacol.* **2018**, *69*. https://doi.org/10.26402/jpp.2018.3.05.
41. Hu, J.; Wu, J.; Liu, X.; Zhang, Y.; Mo, L.; Liu, L.; Liu, S.; Ou, C.; He, Y. Hypoxia enhances autophagy level of human sperms. *Sci. Rep.* **2024**, *14*, 8465. https://doi.org/10.1038/s41598-024-59213-1.
42. Kim, S.T.; Omurtag, K.; Moley, K.H. Decreased spermatogenesis, fertility, and altered Slc2A expression in Akt1-/- and Akt2-/- testes and sperm. *Reprod. Sci.* **2012**, *19*, 31–42.
43. Lee, J.; Kanatsu-Shinohara, M.; Inoue, K.; Ogonuki, N.; Miki, H.; Toyokuni, S.; Kimura, T.; Nakano, T.; Ogura, A.; Shinohara, T. Akt mediates self-renewal division of mouse spermatogonial stem cells. *Development* **2007**, *134*, 1853–1859.
44. Almeida, C.; Cardoso, M.F.; Sousa, M.; Viana, P.; Gonçalves, A.; Silva, J.; Barros, A. Quantitative study of caspase-3 activity in semen and after swim-up preparation in relation to sperm quality. *Hum. Reprod.* **2005**, *20*, 1307–1313.
45. Mohammadi, P.; Mesbah-Namin, S.A.; Movahedin, M. Attenuation of aquaporin-3 may be contributing to low sperm motility and is associated with activated caspase-3 in asthenozoospermic individuals. *Andrologia* **2021**, *53*, e14119.
46. Shin, H.-K.; Bang, Y.-J. Aromatic Amino Acid Metabolites: Molecular Messengers Bridging Immune-Microbiota Communication. *Immune Netw.* **2025**, *25*, e10. https://doi.org/10.4110/in.2025.25.e10.
47. Dodd, D.; Spitzer, M.H.; Van Treuren, W.; Merrill, B.D.; Hryckowian, A.J.; Higginbottom, S.K.; Le, A.; Cowan, T.M.; Nolan, G.P.; Fischbach, M.A.; et al. A gut bacterial pathway metabolizes aromatic amino acids into nine circulating metabolites. *Nature* **2017**, *551*, 648–652.
48. Liu, Y.; Chen, H.; Van Treuren, W.; Hou, B.H.; Higginbottom, S.K.; Dodd, D. *Clostridium sporogenes* uses reductive Stickland metabolism in the gut to generate ATP and produce circulating metabolites. *Nat. Microbiol.* **2022**, *7*, 695–706.
49. Elsden, S.R.; Hilton, M.G.; Waller, J.M. The end products of the metabolism of aromatic amino acids by Clostridia. *Arch. Microbiol.* **1976**, *107*, 283–288.

50. Wu, X.; Xu, J.; Li, J.; Deng, M.; Shen, Z.; Nie, K.; Luo, W.; Zhang, C.; Ma, K.; Chen, X.; et al. Bacteroides vulgatus alleviates dextran sodium sulfate-induced colitis and depression-like behaviour by facilitating gut-brain axis balance. *Front. Microbiol.* **2023**, *14*, 1287271.
51. Wang, P.; Wang, R.; Zhao, W.; Zhao, Y.; Wang, D.; Zhao, S.; Ge, Z.; Ma, Y.; Zhao, X. Gut microbiota-derived 4-hydroxyphenylacetic acid from resveratrol supplementation prevents obesity through SIRT1 signaling activation. *Gut Microbes* **2025**, *17*, 2446391.
52. Wang, A.; Guan, B.; Yu, L.; Liu, Q.; Hou, Y.; Li, Z.; Sun, D.; Xu, H. Palmatine protects against atherosclerosis by gut microbiota and phenylalanine metabolism. *Pharmacol. Res.* **2024**, *209*, 107413. https://doi.org/10.1016/j.phrs.2024.107413.
53. Trott, O.; Olson, A.J. AutoDock Vina: Improving the speed and accuracy of docking with a new scoring function, efficient optimization, and multithreading. *J. Comput. Chem.* **2010**, *31*, 455–461.
54. Lipinski, C.A.; Lombardo, F.; Dominy, B.W.; Feeney, P.J. Experimental and computational approaches to estimate solubility and permeability in drug discovery and development settings. *Adv. Drug. Deliv. Rev.* **2001**, *46*, 3–26.
55. David, L.A.; Maurice, C.F.; Carmody, R.N.; Gootenberg, D.B.; Button, J.E.; Wolfe, B.E.; Ling, A.V.; Devlin, A.S.; Varma, Y.; Fischbach, M.A.; et al. Diet rapidly and reproducibly alters the human gut microbiome. *Nature* **2014**, *505*, 559–563. https://doi.org/10.1038/nature12820.
56. Wastyk, H.C.; Fragiadakis, G.K.; Perelman, D.; Dahan, D.; Merrill, B.D.; Yu, F.B.; Topf, M.; Gonzalez, C.G.; Van Treuren, W.; Han, S.; et al. Gut-microbiota-targeted diets modulate human immune status. *Cell* **2021**, *184*, 4137–4153.e14. https://doi.org/10.1016/j.cell.2021.06.019.
57. Zeevi, D.; Korem, T.; Zmora, N.; Israeli, D.; Rothschild, D.; Weinberger, A.; Ben-Yacov, O.; Lador, D.; Avnit-Sagi, T.; Lotan-Pompan, M.; et al. Personalized Nutrition by Prediction of Glycemic Responses. *Cell* **2015**, *163*, 1079–1094. https://doi.org/10.1016/j.cell.2015.11.001.
58. Berry, S.E.; Valdes, A.M.; Drew, D.A.; Asnicar, F.; Mazidi, M.; Wolf, J.; Capdevila, J.; Hadjigeorgiou, G.; Davies, R.; Al Khatib, H.; et al. Human postprandial responses to food and potential for precision nutrition. *Nat. Med.* **2020**, *26*, 964–973. Correction in *Nat. Med.* **2020**, *26*, 1802. https://doi.org/10.1038/s41591-020-0934-0.
59. Qi, C.; He, G.; Qian, K.; Guan, S.; Li, Z.; Liang, S.; Liu, J.; Ke, X.; Zhang, S.; Lu, M.; et al. gutMGene v2.0: An updated comprehensive database for target genes of gut microbes and microbial metabolites. *Nucleic Acids Res.* **2025**, *53*, D783–D788. https://doi.org/10.1093/nar/gkae1002.
60. Amberger, J.S.; Bocchini, C.A.; Schiettecatte, F.; Scott, A.F.; Hamosh, A. OMIM.org: Online Mendelian Inheritance in Man (OMIM®), an online catalog of human genes and genetic disorders. *Nucleic Acids Res.* **2015**, *43*, D789–D798. https://doi.org/10.1093/nar/gku1205.
61. Davis, A.P.; Wiegers, T.C.; Johnson, R.J.; Sciaky, D.; Wiegers, J.; Mattingly, C.J. Comparative Toxicogenomics Database (CTD): Update 2023. *Nucleic Acids Res.* **2023**, *51*, D1257–D1262. https://doi.org/10.1093/nar/gkac833.
62. Cheng, L.; Qi, C.; Yang, H.; Lu, M.; Cai, Y.; Fu, T.; Ren, J.; Jin, Q.; Zhang, X. gutMGene: A comprehensive database for target genes of gut microbes and microbial metabolites. *Nucleic Acids Res.* **2022**, *50*, D795–D800. https://doi.org/10.1093/nar/gkab786.
63. Lin, Z.; Zhang, Z.; Ye, X.; Zhu, M.; Li, Z.; Chen, Y.; Huang, S. Based on network pharmacology and molecular docking to predict the mechanism of Huangqi in the treatment of castration-resistant prostate cancer. *PLoS ONE* **2022**, *17*, e0263291. https://doi.org/10.1371/journal.pone.0263291.
64. Alamri, M.A.; Tahir ul Qamar, M. Network pharmacology based virtual screening of flavonoids from Dodonea angustifolia and the molecular mechanism against inflammation. *Saudi Pharm. J.* **2023**, *31*, 101802. https://doi.org/10.1016/j.jsps.2023.101802.
65. Liu, Y.; Yang, X.; Gan, J.; Chen, S.; Xiao, Z.-X.; Cao, Y. CB-Dock2: Improved protein–ligand blind docking by integrating cavity detection, docking and homologous template fitting. *Nucleic Acids Res.* **2022**, *50*, W159–W164. https://doi.org/10.1093/nar/gkac394.
66. Laskowski, R.A.; Swindells, M.B. LigPlot+: Multiple ligand–protein interaction diagrams for drug discovery. *J. Chem. Inf. Model.* **2011**, *51*, 2778–2786. https://doi.org/10.1021/ci200227u.

Disclaimer/Publisher's Note: The statements, opinions and data contained in all publications are solely those of the individual author(s) and contributor(s) and not of MDPI and/or the editor(s). MDPI and/or the editor(s) disclaim responsibility for any injury to people or property resulting from any ideas, methods, instructions or products referred to in the content.